A MINIMAL MODEL FOR SPATIO–TEMPORAL PATTERNS IN THIN FILM FLOW

By

H.S. Brown
I.G. Kevrekidis
and
M.S. Jolly

IMA Preprint Series # 790
March 1991

A Minimal Model for Spatio–Temporal Patterns in Thin Film Flow

H.S. Brown and I.G. Kevrekidis
Department of Chemical Engineering, Princeton University
Princeton, NJ 08544

M.S. Jolly
Department of Mathematics, Indiana University
Bloomington, IN 47405

Abstract

We consider the development of spatio–temporal oscillations in the Kuramoto–Sivashinsky amplitude model of thin film flow. These develop from Hopf bifurcations off of steady state solutions and are observed to undergo symmetry breaking and period doubling bifurcations. Oscillatory branches in the parameter regime studied apparently terminate in Silnikov type homoclinic connections. A minimal, three mode nonlinear Galerkin discretization, capable of capturing this bifurcation behavior is constructed. A simple shooting algorithm which exploits this sharp reduction in dimensionality is used to accurately locate the homoclinic connections.

Key words: Kuramoto–Sivashinsky equation, Silnikov connections, symmetry breaking, inertial manifolds.

1 Introduction

The Kuramoto–Sivashinsky equation (KSE) [27, 36]

$$v_t + 4v_{xxxx} + \alpha(vv_x + v_{xx}) = 0. \tag{1}$$

has been used as an amplitude equation to describe incipient instabilities in several physical contexts. It can be derived from a long–wave perturbation analysis of the two dimensional Navier–Stokes Equations describing the flow of a thin, viscous liquid film with surface tension, flowing down a vertical plane. The equation has been the subject of numerous theoretical and computational studies during the last fifteen years (e.g. [21, 9, 26, 19] and references therein) probably because of its ability to exhibit low–dimensional, spatially coherent but temporally complicated solution patterns. Numerical simulations have uncovered a wealth of such patterns, ranging from steady states, periodic oscillations and traveling waves to modulated traveling waves, symmetry–driven persistent homoclinic loops, and complicated (apparently chaotic) dynamics as the instability parameter α grows. Theoretical work based largely on symmetry considerations has concentrated on steady state and traveling wave solutions, as well as heteroclinic and homoclinic connections between them (e.g. [1]).

In this work we concentrate on the computer assisted study of limit cycle (time periodic) solution branches arising from low α Hopf bifurcations. Two types of periodic solutions are observed, one possessing a spatio–temporal symmetry that relates the first half of the period of the oscillation with the second half. Such a symmetry is known to suppress period doubling of the oscillations [38]. A symmetry breaking pitchfork bifurcation follows, with subsequent period doublings of the non-symmetric limit cycles. All oscillatory branches apparently terminate on Silnikov type infinite period homoclinic connections (heteroclinic connections for the symmetric limit cycles), involving saddle type steady state solutions. While Silnikov saddle connections can occur in a phase space of dimension three, the simple three mode Galerkin truncation of the PDE (1) cannot capture these phenomena. However, using the theory of approximate inertial manifolds, we construct a minimal (three dimensional) *nonlinear* Galerkin discretization which qualitatively (and to some extent quantitatively) captures the Silnikov behavior in the parameter regime studied. This sharp reduction in the dimensionality of the problem

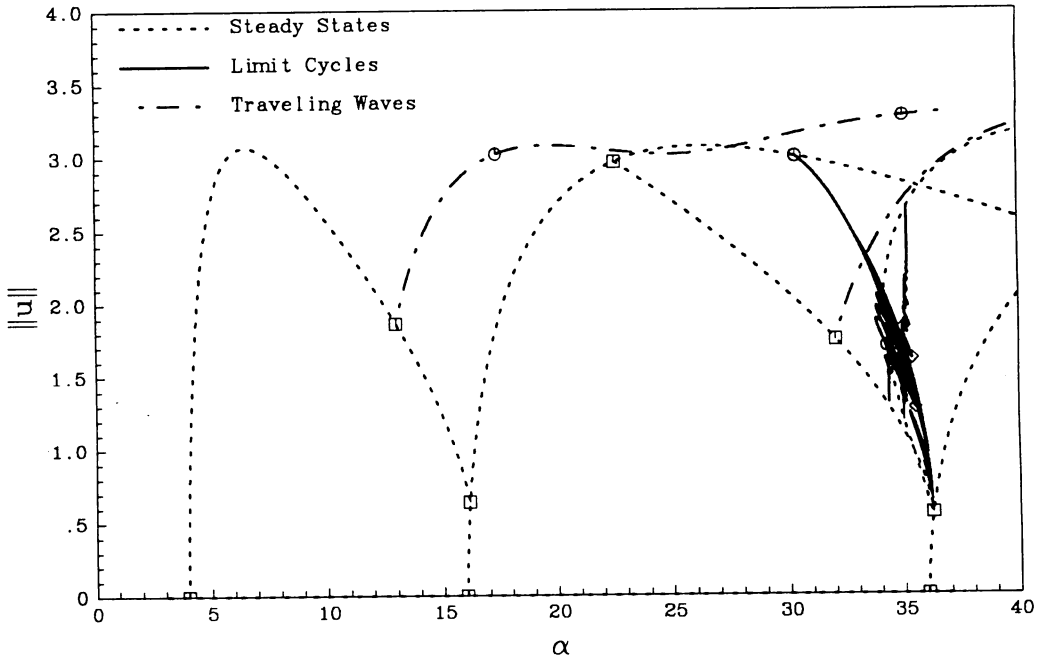

Figure 1: Bifurcation diagram for the KSE; □ marks steady state and traveling wave bifurcations; o marks Hopf bifurcation points.

allows for the easy visualization of the stable and unstable manifolds involved in these interactions. We have exploited this to implement a simple shooting algorithm which converges on the Silnikov loop in (phase × parameter) space.

2 Numerical Bifurcation Diagrams

Figure 1 is a bifurcation diagram for the KSE for $0 < \alpha < 40$. The diagram shows steady, periodic, and traveling wave solution branches computed using a traditional Galerkin spectral discretization of the PDE with nine Fourier modes. The diagram is "converged" in the sense that doubling the dimension of the discretization does not visibly alter the location or the stability of the solution branches.

Our calculations were actually performed using the integrated form of the

KSE with periodic boundary conditions on $0 < x < 2\pi$:

$$u_t + 4u_{xxxx} + \alpha\left(\frac{1}{2}(u_x)^2 + u_{xx} - \frac{1}{4\pi}\int_0^{2\pi}(u_x)^2\,dx\right) = 0. \qquad (2)$$

AUTO, a continuation/bifurcation package developed by E. Doedel [12, 13] was used to perform these calculations. The steady state and limit cycle branches (the latter are often called "standing waves") were calculated by restricting the dynamics to the invariant subspace of even functions; all subsequent calculations in this paper will be similarly restricted. Until recently most of the rigorous results (dissipativity, existence and dimension estimates for inertial manifolds) for the KSE have been limited to this invariant subspace (see for example [33]). Il'yashenko [22] has recently presented a proof of dissipativity for the general case of periodic boundary conditions. The traveling wave branches, computed in full Fourier space with periodic boundary conditions, are included here for completeness. Another form of solution (modulated traveling waves) also known to exist in the full Fourier space within this parameter range have not been included in the diagram, since the discussion will be mostly restricted to even solutions and their bifurcations. Such bifurcation diagrams, particularly those including the steady state solutions of the KSE have appeared in the literature (e.g. [34, 19, 3]). In this paper we focus on the family of limit cycle branches observed for $30 < \alpha < 37$. Certain aspects of these branches and their bifurcations have been discussed previously in [24, 23, 7].

The steady state branches bifurcating at $\alpha = 4(= 4{*}1^2), 16(= 4{*}2^2), 36(= 4 * 3^2), \ldots 4 * k^2$ are characterized as "unimodal" ($k = 1$), "bimodal" ($k = 2$), ... "k-modal" respectively, based on their spatial structure close to the respective bifurcations. A Hopf bifurcation occurs at $\alpha \sim 30.34$ off of the bimodal steady state branch (restricted on the invariant subspace of even functions). This limit cycle with period T (i.e. $u(x,t) = u(x,t+T)$) is characterized by a spatio–temporal symmetry: the second half period of the oscillation (in time) is related to the first half period by:

$$u(x,t) = u(x+\pi, t+T/2).$$

This symmetry is a version of what Aronson *et al.* call "Ponies On a Merry-go-round" for discrete arrays of Josephson junctions [2]. The implications of such a symmetry on the bifurcation behavior of periodic solutions was discussed by Swift and Wiesenfeld [38].

To understand the properties of these symmetric limit cycles, it is helpful to consider certain replication and invariance properties of the solutions of the KSE. It is easy to see that the space

$$C_k \equiv \text{span}(\cos(kx), \cos(2kx), \cos(3kx) \ldots)$$

is invariant under the flow of the KSE and that if $u(x,t)$ is a solution of the KSE for some parameter value α_0, then so is $u(kx, k^4 t)$ at $\alpha = k^2 \alpha_0$. This means that steady state branches of the KSE replicate as discussed in detail in [34]. For every nontrivial steady state branch, a one–parameter family of steady states exists at every α value, each one of them a shift (in x) of the others. All steady state branches shown in figure 1 (unimodal, bimodal, trimodal, as well as a mixed mode branch, the "bi–tri"), represent solutions which can be shifted to be even (i.e. can be represented by a cosine series on $[0, 2\pi]$). Applying the above replication property with $k = -1$, we see that two "representatives" of each nontrivial k–modal steady state branch can be found in C_k, related to each other by a translation by π/k. The bi–tri steady state branch can be thought of as "unimodal" in this context: two representatives of it exist in C_1 related to each other by a translation by $\pi/1$.

We are interested here in the bifurcations of these even solutions, taking place in the invariant subspace of even functions. The two representatives of odd–modal ($k = 1, 3, 5, \ldots$) branches can be shown to have the same stability in C_1; on the other hand, the two representatives of even–modal ($k = 2, 4, 6, \ldots$) branches have different stability properties in C_1 (while of course they have the same stability in C_k as well as in the full Fourier space, where they also both possess a zero eigenvalue corresponding to the direction of shift invariance). The Hopf bifurcation observed at $\alpha \sim 30.34$ is not a replication of a lower α Hopf bifurcation on the unimodal branch. Since the eigenvalues (eigenvectors) of the bimodal representatives in C_2 are identical (replicas) to those of the unimodal representatives in C_1, this Hopf bifurcation does not occur entirely *within* C_2 and hence involves components in C_1, in which the stability of the two bimodal representatives is different. The Hopf bifurcation is therefore expected to (and indeed observed to) occur for only one of the two representatives of the bimodal branch.

We now restrict our analysis to the invariant subspace of even functions C_1. The two bimodal representatives are each invariant under π shifts and transformed into each other by $\pi/2$ shifts. Since the replication law with

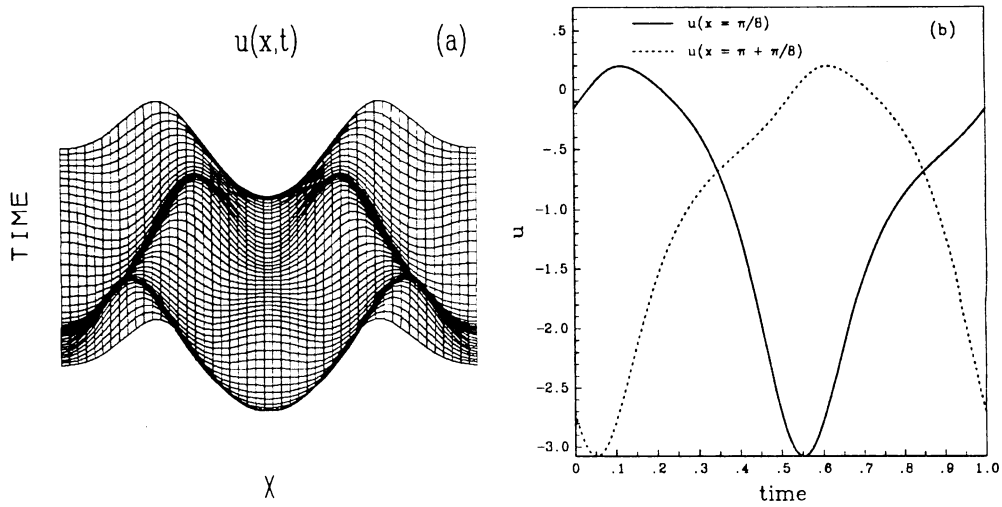

Figure 2: (a) A space–time plot of one period of a symmetric limit cycle ($0 < x < 2\pi$) at $\alpha \sim 33.56$. (b) Time series of the amplitude at $x = \pi/8$ and $x = \pi + \pi/8$ during one period of the oscillation.

$k = -1$ (the shift by π) is a property of both steady and time dependent solutions, the unique limit cycle resulting from the single representative Hopf bifurcation must be (as a solution) invariant to a spatial shift by π. In this case, the spatio–temporal symmetry:

$$u(x) \to S_\pi u(x); \quad t \to t + T/2$$

results, where

$$S_\pi u(x) \equiv u(x + \pi).$$

The symmetry of the limit cycles is illustrated in figure 2. To see how this symmetry will appear in Fourier space, consider the ODE system

$$\dot{a}_n = F_n(\boldsymbol{a}); \;\; n = 1, \ldots, N$$

arising from the Fourier–Galerkin discretization of the KSE:

$$u(x,t) \sim \sum_{n=1}^{N} (u(x,t), \cos(nx)) \cos(nx) \equiv \sum_{n=1}^{N} a_n(t) \cos(nx).$$

The notation $(\cdot, \cdot)$ refers to the standard inner product on L^2. Figure 3 shows a representative phase portrait and time series characteristic of the

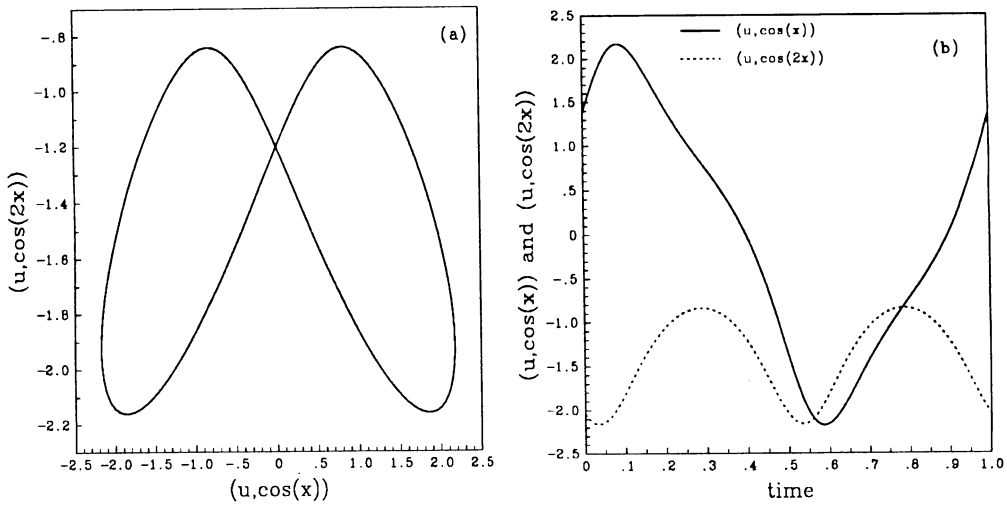

Figure 3: (a) An a_1–a_2 phase space projection of a symmetric limit cycle at $\alpha \sim 33.56$ and (b) time series of two of its Fourier coefficients (a_1 and a_2).

symmetric oscillations. This type of symmetry in limit cycles is known to cause suppression of period doubling. The proof for the KSE follows directly the arguments of Swift and Wiesenfeld, substituting $u(x)$ for their x and S_π (the π shift) for their $-\boldsymbol{I}$. It is also easy to see that the argument carries over for the ODE system resulting from the Galerkin spectral discretization of the PDE. The symmetry becomes

$$\begin{bmatrix} a_1 \\ a_2 \\ a_3 \\ a_4 \\ \cdot \\ \cdot \end{bmatrix} \rightarrow \begin{bmatrix} -a_1 \\ a_2 \\ -a_3 \\ a_4 \\ \cdot \\ \cdot \end{bmatrix}, \quad t \rightarrow t + \frac{T}{2}.$$

In this case, instead of the Swift and Wiesenfeld matrix $-\boldsymbol{I}$, the diagonal matrix $\boldsymbol{J}$ with elements $j_{ii} = (-1)^i$ is used. The basic argument is that for symmetric orbits, the state transition matrix DP is the square of another matrix $(D\hat{P})^2$ and therefore has as eigenvalues the squares of the eigenvalues of the matrix $D\hat{P}$. The matrices being real precludes DP from having a single real eigenvalue crossing the unit circle at -1 as α varies.

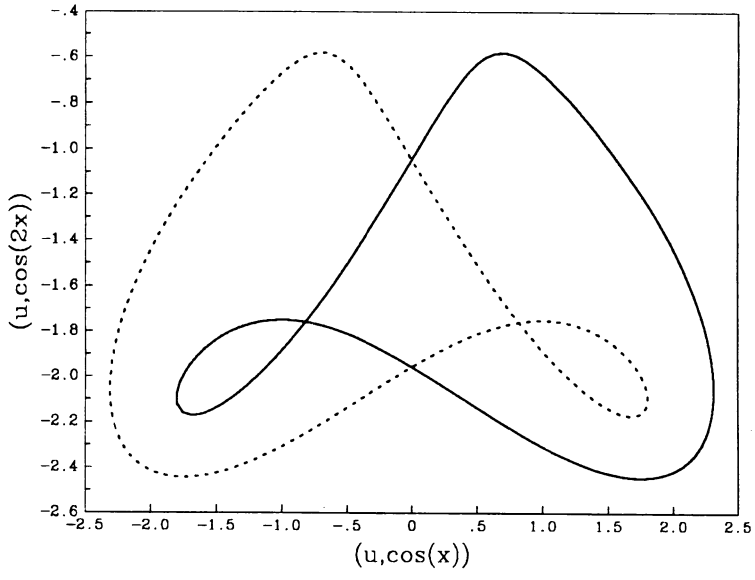

Figure 4: An a_1–a_2 phase space projection of an asymmetric limit cycle and its π shift at $\alpha \sim 33.56$.

In the KSE (as well as in other systems with this property) a symmetry breaking (pitchfork) bifurcation occurs off of the symmetric limit cycle branch at $\alpha \sim 32.85$, giving rise to two "asymmetric" limit cycle branches (symmetric *to each other* by the π shift in x). These are illustrated in figure 4. The asymmetric limit cycles are not prevented from period doubling, and are indeed observed to subsequently undergo a period doubling cascade [23]. The first period doubling occurs at $\alpha \sim 32.97$ and the second at $\alpha \sim 32.99$. Figure 5 shows representative phase portraits of limit cycles on these branches.

These symmetry properties play a significant role in "orchestrating" the complicated structure of limit cycle branches and associated Silnikov connections shown enlarged in figure 6. Partial observations of this intricate pattern have been presented and published previously in [25, 24, 23, 7, 8]; in what follows we attempt a more coherent discussion of the detailed bifurcation picture. Figure 7a shows the fate of both asymmetric limit cycle branches; after the first period doubling, the asymmetric branches undergo a "corkscrew" sequence of turning point bifurcations while their period (not

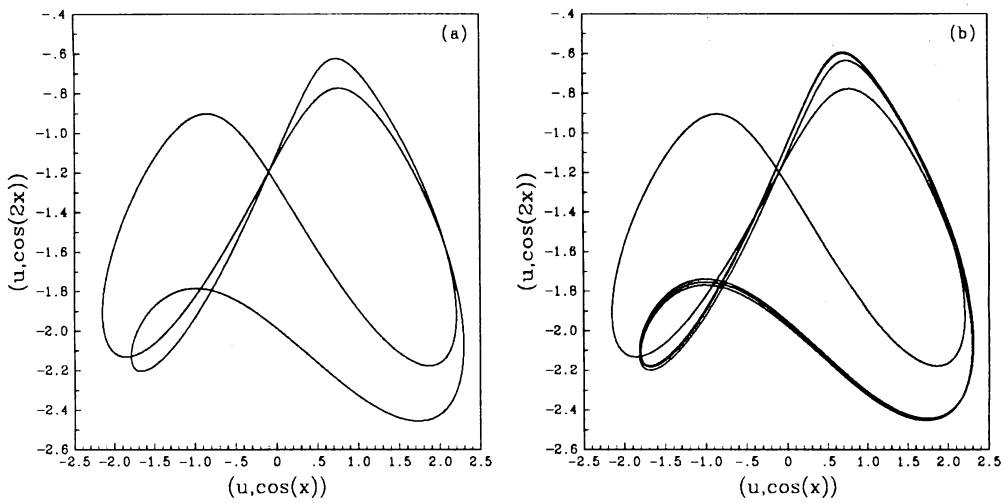

Figure 5: a_1–a_2 phase space projections of (a) the period 2 and (b) the period 4 asymmetric limit cycles at $\alpha \sim 33.56$.

shown in the figure) approaches infinity. In the figure, the branch is seen to asymptotically approach the bi–tri steady state solution branch. This behavior is typical of a homoclinic connection to a saddle–focus (a Silnikov loop). A detailed discussion of the bifurcation behavior associated with this phenomenon in three space dimensions (a one dimensional unstable manifold connecting with a two dimensional stable manifold corresponding to a complex eigenvalue pair) can be found in [18] (see also [17]). A space–time plot and a Fourier space projection of a representative limit cycle close to the "tip" of the corkscrew (figures 7b and c) illustrate the geometry of this connection: the limit cycle is indeed seen to approach (and spend most of its period in the neighborhood of) the bi–tri saddle type steady state. The nature of the eigenvalues of this steady state (confirmed by independent computations) is also obvious in the figure: one is positive and real, while the two least stable eigenvalues of the saddle form a complex conjugate pair (indicated by the spiraling close to the steady state). The limit cycle branch is expected to corkscrew on its approach to homoclinicity if the Silnikov condition, $|\delta| < 1$, is satisfied; δ is the ratio of the real part of the complex eigenvalue pair to the real eigenvalue of the saddle–focus (see [18]). A number of other features, qualitatively and quantitatively predicted in the Glendinning and Sparrow

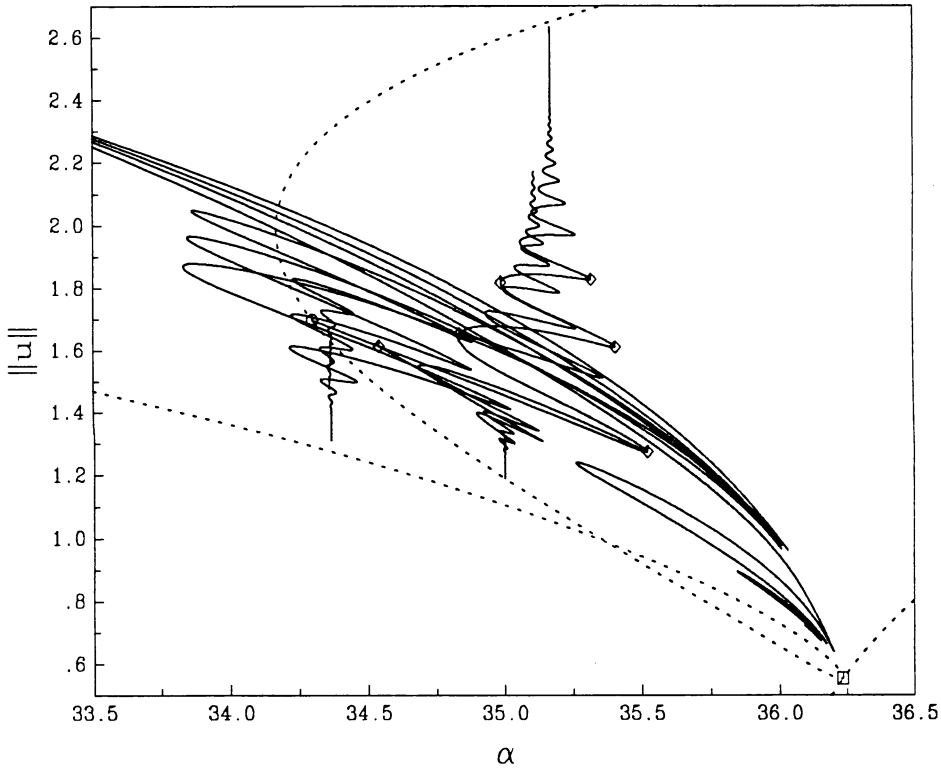

Figure 6: Enlarged bifurcation diagram for the KSE. □ marks steady state bifurcations, ○ marks Hopf bifurcation points, and ◇ marks period doubling bifurcations.

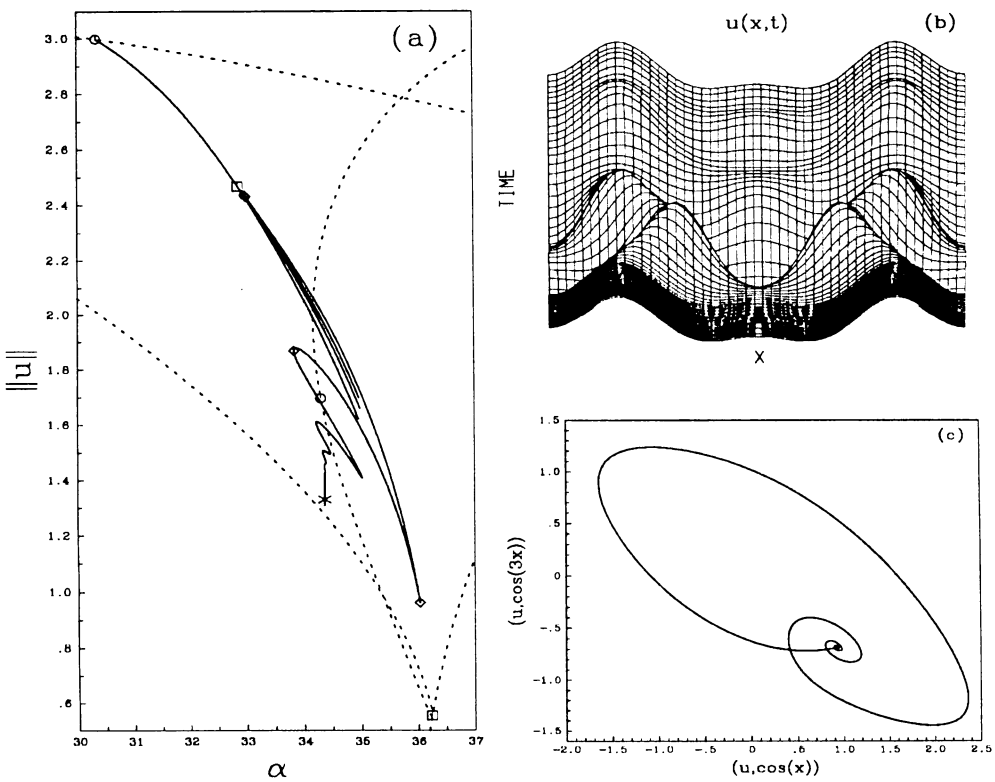

Figure 7: (a) Partial bifurcation diagram of the asymmetric limit cycle branch. (b) Space–time plot and (c), an a_1–a_3 phase space projection of a limit cycle approaching homoclinicity ($\alpha \sim 34.37$, marked with a *).

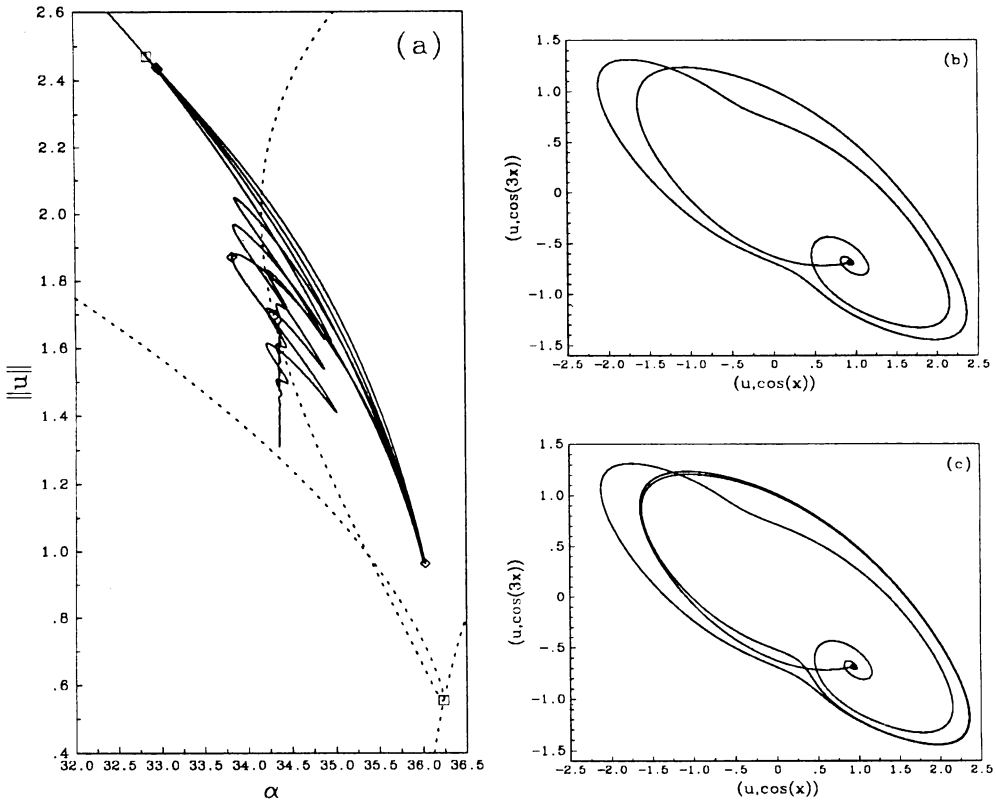

Figure 8: (a) Partial bifurcation diagram of the asymmetric limit cycle branches. a_1–a_3 phase space projections of the period–2 (b) and period–4 (c) asymmetric limit cycles close to homoclinicity ($\alpha \sim 34.36$).

analysis have also been computationally observed, and are partly seen in this figure (for a better illustration see figure 10). These include the (asymptotically exponential) narrowing of the parameter interval between successive turning points on the corkscrew, the existence of period doubling bifurcations and their relative location with respect to the turning points as well as subsidiary homoclinicities.

Figure 8a overlays the fate of the initial period–doubled and the subsequent period–quadrupled limit cycle branches on figure 7a. We observe that they also asymptotically approach corkscrews located close to that of the primary asymmetric oscillations. Figures 8b and c show Fourier space pro-

jections of representative limit cycles close to the tips of the corresponding corkscrews, indicating again an interaction between the stable and unstable manifolds of the same branch of bi–tri saddle type steady state solutions. Period doubling bifurcations like those on the primary branch are also expected close to the limit points of these subsidiary corkscrews.

Figure 9 shows the fate of the original symmetric limit cycle branch. Computations of this branch also display the beginnings of a corkscrew behavior. However, as the Fourier space projection portraits of representative limit cycles on this branch indicate (figures 9b and c), the limit cycles appear to asymptote towards a symmetric heteroclinic connection. This connection apparently involves the unstable manifold of one saddle type steady state with the stable manifold of its π shift and vice-versa. The computation of this branch presents certain numerical difficulties since the computed limit cycles are very unstable (typical Floquet multipliers even before the first turning point become so large $-O(10^{10})$ and more– as to be inaccurate). These phase portraits are strongly reminiscent of the structure of the Lorenz attractor, and the bifurcation behavior of orbits of this nature has been discussed in Sparrow's book [37].

A much more "textbook" example of Silnikov type behavior is exhibited by the limit cycle branches emanating from the Hopf bifurcation point at $\alpha \sim 34.30$ on the bi–tri steady state branch. The two representatives of this branch have the same stability in the C_1 space and therefore two Hopf bifurcations occur simultaneously, giving rise to two (symmetric to each other) limit cycle branches. Because there are no symmetry restrictions, these branches can (and indeed are observed to) period double according to the typical Silnikov scenario. An initial period doubling at $\alpha \sim 34.54$ results in a limit cycle branch which, as seen in figure 10a, apparently asymptotically approaches a Silnikov connection of a saddle focus on the "middle" (in the figure) steady state branch. A second period doubling at $\alpha \sim 35.52$ gives rise to a branch with a similar fate. Interestingly the next period doubling on the "primary" corkscrew ($\alpha \sim 34.84$) gives rise to a period doubled branch which appears to asymptotically approach a homoclinic connection of a saddle lying on a different part of the steady state branch. This is a "subsidiary homoclinicity" and a representative limit cycle portrait on this branch (figure 10c) clearly illustrates closeness to a "double pass" Silnikov connection (as opposed to the "single pass" of the primary homoclinicity (figure 10b).

Obviously the details of these diagrams are incomplete –one could go

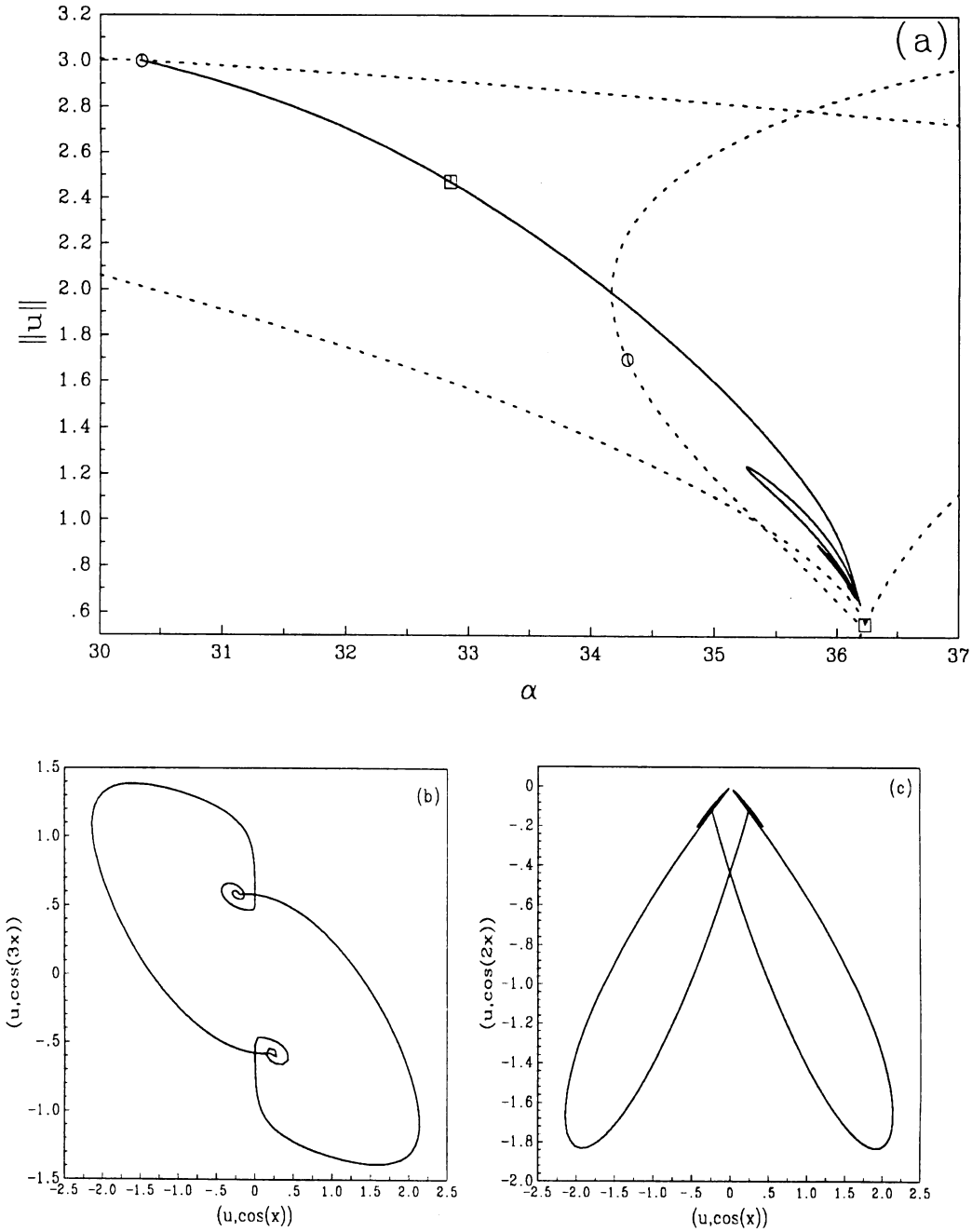

Figure 9: (a) Partial bifurcation diagram of the symmetric limit cycle branch. (b) a_1–a_3 and (c) a_1–a_2 phase space projections of a representative limit cycle ($\alpha \sim 36.15$).

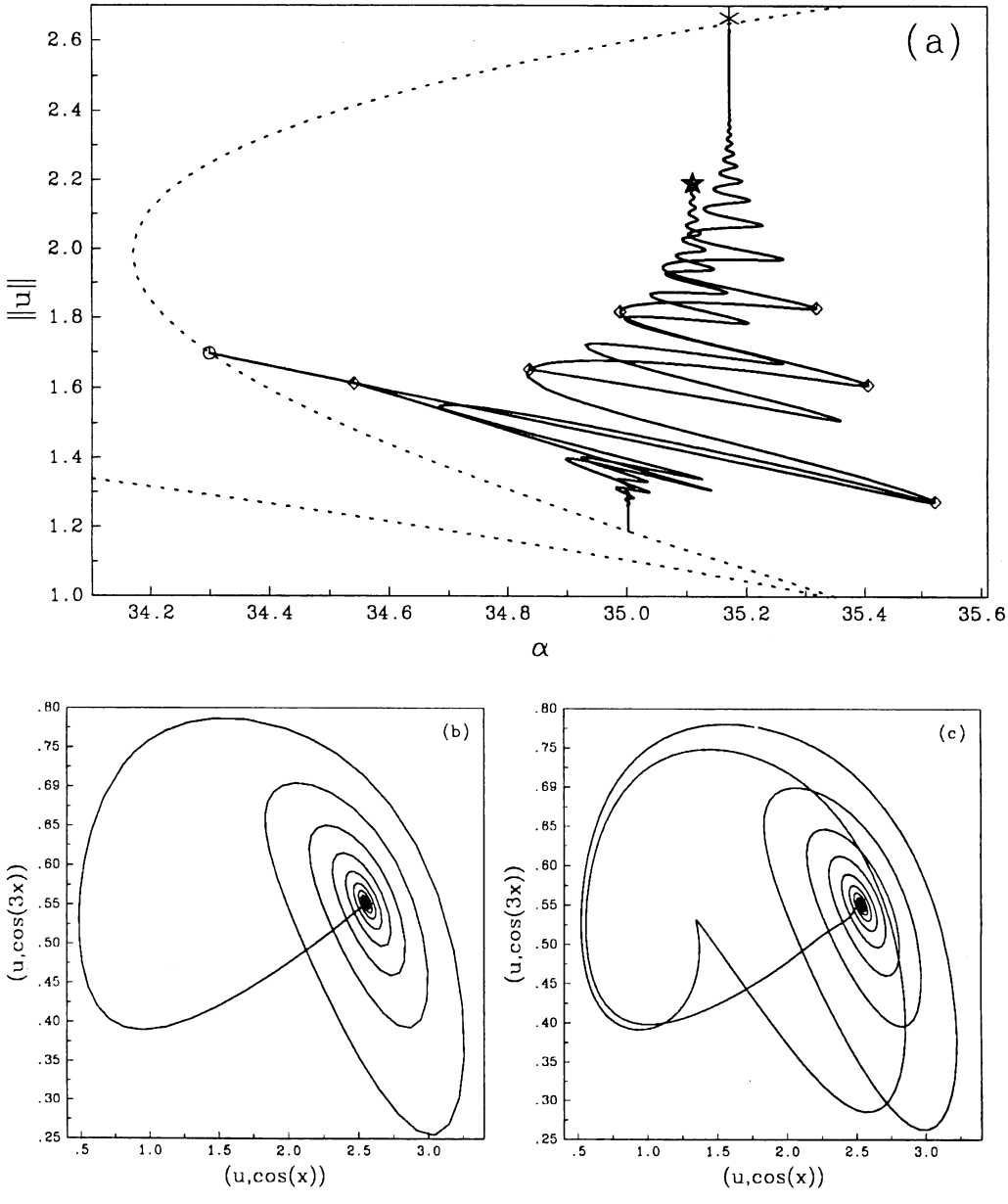

Figure 10: (a) Partial bifurcation diagram of the limit cycle branches bifurcating from the bi–tri steady state branch. (b) and (c) show phase space projections of a period 1 ($\alpha \sim 35.17$, marked with a *) and a period 2 ($\alpha \sim 35.11$, marked with a $\star$) limit cycle approaching homoclinicity.

on computing limit points, period doublings, and subsequent homoclinicities forever. It is sufficient to summarize this entire scenario as a form of "loss of a limit cycle branch" [18]. Before concluding this descriptive section, we should add that even this complicated scenario does not contain all essential features of the dynamics of the KSE in C_1 in the parameter interval studied; Simulations indicate additional global bifurcations for even earlier values of α than the ones discussed here (e.g. close to $\alpha = 32.9000355$); the picture is far from being complete.

3 An accurate three mode model

The bifurcation calculations in the previous section were performed using a nine mode traditional Galerkin spatial discretization of the PDE. While the computational task involved in this level of analysis for nine ODEs is tractable, it is conceivable that an alternative discretization technique could capture the dynamics accurately with a smaller number of modes. A traditional approach to model reduction, particularly suitable for the qualitative local analysis of bifurcating branches, involves studying the flow on a center manifold in the neighborhood of a particular bifurcating solution. An example of this type of analysis for the KSE in the recent literature can be found in [1]. An alternative approach involves Galerkin projection on empirically determined basis functions obtained from statistical processing of computationally or experimentally obtained time series. This more practically oriented approach (method of empirical eigenfunctions or Proper Orthogonal Decomposition, POD), introduced by Lumley [30, 31] as a method of detecting spatially coherent structures in turbulence, has been extensively used in recent years for the study of transitional flows in various geometries (e.g. [4, 35, 11]) and references therein).

A *global* (in phase space) model reduction approach is motivated by the theory of inertial manifolds. This theory can be described for a dissipative PDE written as an evolutionary equation in a Hilbert space H

$$\frac{du}{dt} + Au + F(u) = 0, \quad u \in H.$$

For example, for the KSE we let $A = \frac{\partial^4}{\partial x^4}$ and

$$F(u) = \alpha \left(\frac{\partial^2 u}{\partial x^2} + \frac{1}{2} \left(\frac{\partial u}{\partial x} \right)^2 - \frac{1}{4\pi} \int_0^{2\pi} (u_x)^2 \, dx \right).$$

An inertial manifold is a finite dimensional, positively invariant, exponentially attracting Lipschitz manifold embedded in the phase space H. Let $P = P_m$ denote the orthogonal projector onto the span of the first m eigenfunctions of A, and let $Q = Q_m = I - P_m$ be that onto the orthogonal complement. Typically an inertial manifold is constructed as the graph of a function $\Phi : PH \to QH$. This function is used to define a finite dimensional ODE (the inertial form)

$$\frac{dp}{dt} + Ap + PF(p + \Phi(p)) = 0, \quad p \in PH$$

which captures all the long time behavior of the PDE.

While inertial manifolds are known to exist for the KSE as well as other dissipative PDEs (see e.g. Constantin *et al.* [10]), they cannot in general be expressed in closed form. For this reason a number of approximate inertial manifolds (AIMs) have been introduced in the literature (see [32] and the references therein). The AIM used here is designed to pass near all steady states of the PDE, which lie on the global attractor, and consequently on any inertial manifold. This construction is also well motivated for dissipative PDEs that may not necessarily possess an inertial manifold. Indeed, this AIM was originally introduced in [39] for the Navier-Stokes equations (NSE). Consider the Q-component of the condition for a steady state

$$Aq + QF(p + q) = 0, \quad p \in PH, \; q \in QH,$$

which implicitly defines an analytic function $\Phi^s : PH \to QH$ given by the fixed points for the family of mappings

$$T_p(q) = -A^{-1} QF(p + q),$$

provided m is large enough. The AIM used in computations in this paper

$$\Phi_2(p) \equiv T_p(T_p(0))$$

has a distance to Φ^s (in L^2) which is comparable to that between Φ^s and the global attractor (see [39] for the NSE, [23] for the KSE).

The implementation of this nonlinear Galerkin approximation is well suited for computation using spectral methods. The nonlinear Galerkin method used here i.e. the m dimensional ODE system

$$\frac{dp}{dt} + Ap + PF(p + \Phi_2(p)) = 0, \qquad p \in PH, \tag{3}$$

(called an Approximate Inertial Form, AIF) amounts to three successive evaluations of the nonlinearity F. For the KSE, with its quadratic nonlinearity and periodic boundary conditions, the graph of Φ_2 lives in the span of the first $4m$ eigenfunctions of A (Fourier modes, cosines for the even functions here). This means that with sufficient padding with zeros, spectral codes can be used to compute the vectorfield of (3) faithfully. In the general case where the nonlinearity is not of polynomial type, a collocation scheme can be implemented efficiently using the Fast Fourier Transform, albeit with aliasing errors [7].

Obviously, the minimal number of modes (phase space dimension) necessary to accommodate the Silnikov loop phenomena described above, is three. However, a traditional three mode Galerkin discretization does not capture these phenomena [23]. The best *a priori* estimates for the dimension of an inertial manifold for the KSE do not suggest that this dimension could be as low as three or, for that matter, even nine (which we empirically know to be sufficient from our computational results). Our choice here of the dimension of the approximate inertial manifold (three) is therefore based on the dynamic phenomena observed rather than on rigorous estimates.

Figure 11 shows the relevant section of the bifurcation diagram for the AIF (3) with three modes, which does indeed exhibit the same limit cycle bifurcation behavior as the "converged" diagram (figure 6). The original Hopf bifurcation from the bimodal branch to a symmetric limit cycle, the subsequent symmetry breaking followed by period doublings, as well as the ultimate Silnikov loop terminations of the resulting branches are present (we had some numerical difficulties with the extensive continuation of the symmetric limit cycle branch). Similarly, the "nonsymmetric" limit cycle branches bifurcating off of the bi–tri mixed mode steady state branch, their subsequent period doublings, Silnikov loops, and subsidiary homoclinicities are correctly (and, to some extent, accurately) reproduced. The actual parameter val-

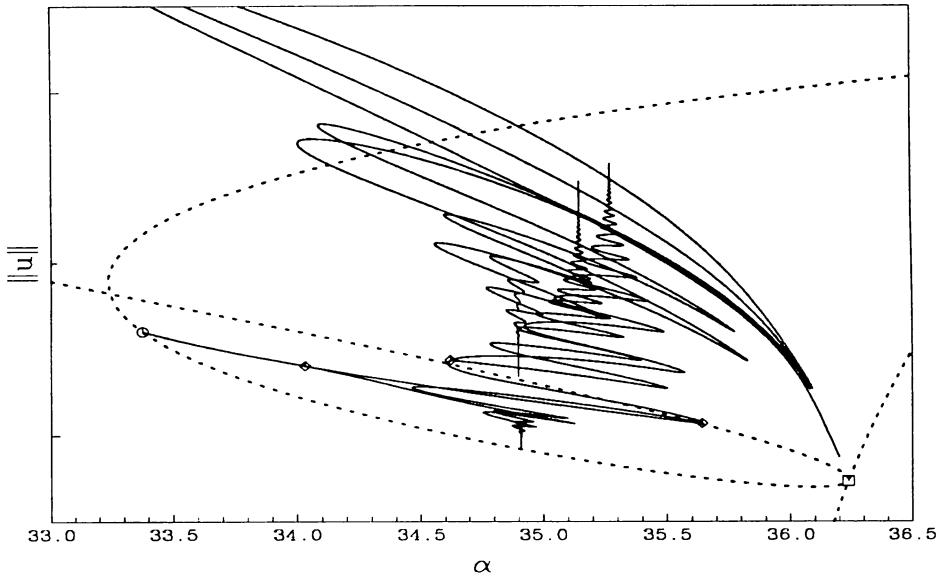

Figure 11: Partial bifurcation diagram for the KSE obtained using the AIF (3) with $m = 3$.

ues at which the Silnikov connections occur in the reduced system are not identical to the traditional Galerkin values; however, they are in reasonable semi–quantitative agreement.

4 Approximating the Silnikov connections

The existence of certain Silnikov type homoclinic connections "implies" the existence of a complicated pattern of bifurcations and oscillatory branches in the neighborhood of these connections in (phase $\times$ parameter) space. Several aspects of this scenario were illustrated above for the KSE. On the other hand, this entire bifurcation sequence can be thought of as a mechanism for the disappearance of the "primary" limit cycle branch as the bifurcation parameter changes. For example, the collection of limit cycle branches around $\alpha \sim 35.17$ in figure 10 can be taken to simply denote the "death" of the nonsymmetric limit cycle branch originating at $\alpha \sim 34.30$.

The continuation of limit cycle branches as they approach homoclinicity involves considerable computational effort without necessarily producing sig-

nificant information. Due to its infinite complexity, the diagram can never be completed; in addition, as the limit cycle branches approach homoclinicity their period approaches infinity, and their accurate calculation poses severe discretization problems. On the other hand, all these complications occur in a very narrow parameter interval, and it appears that approximating the Silnikov connection directly would for all practical purposes contain the essential information regarding the behavior of the limit cycle branch(es).

Figure 7c is representative of the phase space geometry of a Silnikov connection. The one dimensional unstable manifold of a saddle steady state connects with the saddle itself (and therefore lies on the stable manifold). The spiraling approach to the saddle is indicative of the complex conjugate nature of the two least stable saddle eigenvalues ("saddle–focus"). This figure is of course only a projection, and the stable manifold is not two dimensional, as was the case in Glendinning and Sparrow (for this figure it is actually eight dimensional). The model reduction approach discussed in section 3 reduces the dimensionality of the stable manifold to two, the minimum necessary, and allows for the easy visualization of both invariant manifolds and their interactions. We have used this reduction to implement a geometrically motivated simple shooting algorithm to converge on the Silnikov loop. Such algorithms (special cases of boundary value problems on semi–infinite or infinite intervals [29]) have appeared in the literature for the calculation of saddle connections in low dimensional systems [20] (see [28] for the Silnikov case). More recently, results for the general case with arbitrary (finite) dimensional interacting manifolds have been reported [14, 15, 16, 6, 5].

We now present an outline of our implementation for the case when the associated steady state has a one dimensional unstable manifold and a two dimensional stable manifold. For simplicity we rewrite the approximate inertial form (3) as

$$\dot{p} = G(p; \alpha). \tag{4}$$

Let $\hat{p}(\alpha)$ denote a fixed point of (4) with associated stable eigenvector $v_1 \pm i v_2$ and unstable eigenvector v_3. Let C_r define a cylinder of radius r with its axis in the direction of v_3 passing through the point $\hat{p}$. Consider also the plane spanned by the vectors v_1, v_2 passing through $\hat{p}$ (see figure 12). Given a good guess α_n for the parameter value, α^*, at which the Silnikov loop occurs, the computational procedure is outlined below:

1. Locate the steady state $\hat{p}(\alpha_n)$ via Newton iteration and compute its

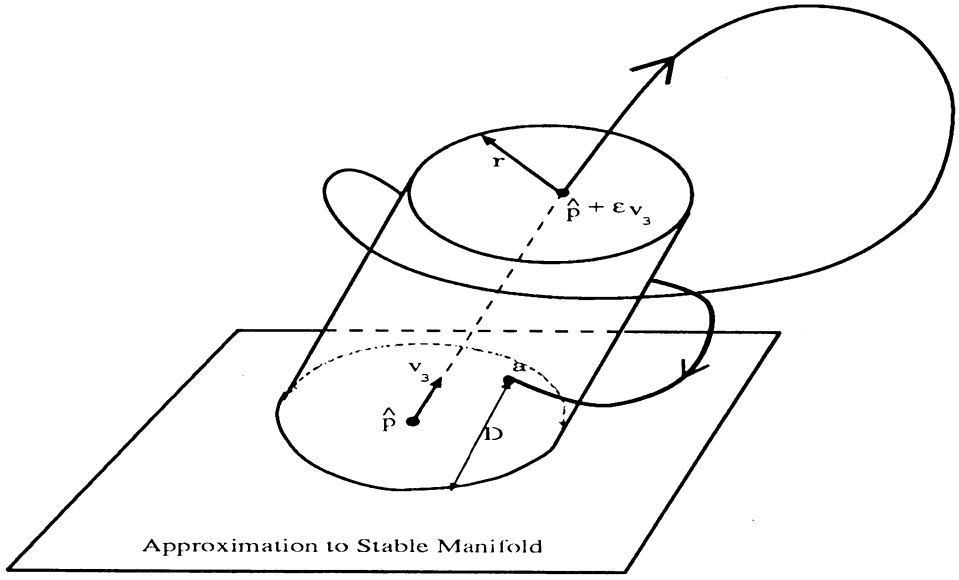

Figure 12: Illustration of the geometry and terminology used in the shooting algorithm.

eigenvectors.

2. Integrate

$$\begin{aligned} \dot{p} &= G(p; \alpha_n) \\ p(t=0) &= \hat{p} + \epsilon v_3 \end{aligned}$$

until the trajectory intersects the cylinder C_r as shown in figure 12. Let a denote the intersection point.

3. Calculate the distance $D = D(\alpha_n, \epsilon, r)$ from a in the direction of v_3 to the plane. To satisfy $D(\alpha) = 0$:

4. Calculate the derivative $\frac{dD}{d\alpha}$ and use it to update the current guess for α via a Newton iteration:

$$\alpha_{n+1} = \alpha_n - \left[\frac{dD}{d\alpha}\right]^{-1}_{\alpha_n} D|_{\alpha_n}.$$

Upon convergence of this procedure we obtain an $\alpha(\epsilon, r)$ satisfying $D(\alpha, \epsilon, r) \sim 0$. Since v_3 is tangent to the unstable manifold at $\hat{p}$, it is obviously a good approximation of the unstable manifold for small enough ϵ. Similarly, the plane provides a good approximation of the stable manifold for small r. Therefore, in the limit, $\alpha(r, \epsilon)$ should approximate α^*. In our implementation we have repeated the above procedure by systematically shrinking r and ϵ until $\alpha(\epsilon, r)$ remains constant to within a prescribed error tolerance (usually $< 10^{-8}$).

Calculation of the intersection point a involves a Newton–Raphson iteration ensuring that it lies on C_r, which implicitly defines the "time of flight" of the trajectory, and can be used to calculate its dependence on the system parameters. The most involved segment of the computational procedure is the evaluation of the derivative $\frac{dD}{d\alpha}$. D depends on α both explicitly through the vectorfield and implicitly through the initial condition (the fixed point and its eigenvectors) and the cylinder itself (again depending on the eigenvectors). The calculation therefore involves repeated application of the chain rule, using information from integration of the sensitivity equations (dependence of the flow on α). It is of course possible to use numerical derivatives in this calculation. Because of the complexity of the implicit differentiations involved in computing the "true" derivatives, we preferred to use *linear* approximations to the stable and unstable manifolds, and progressively "squeeze" them very close to the saddle (where they become increasingly accurate), as opposed to higher order approximations to the local manifolds as in [20, 28]; these approximations are more accurate further away from the saddle, but evaluating their dependence on the parameter becomes increasingly complicated.

Figure 13 shows the convergence rate of the Newton iteration for the location of the Silnikov connection at $\alpha \sim 35.2741195$. The "elbows" in the graph correspond to changes in r. The figure has been obtained by letting $D(\alpha, \epsilon, r)$ approach zero to within 10^{-6} before shrinking the cylinder. Upon convergence of the iteration for a prescribed value of r, the new r has been chosen by allowing the last computed trajectory to further approach the fixed point as close as possible before it starts moving away from it. The reason for not immediately starting with a very small (accurate) r is that simple shooting may fail to return to the cylinder if the initial guess of α is not very accurate. This probably means that convergence for multiple shooting or collocation discretizations for the boundary value problem would be easier. Friedman and Doedel, in a series of papers [14, 15, 16], have discussed various issues associated with computing homoclinic and heteroclinic connections be-

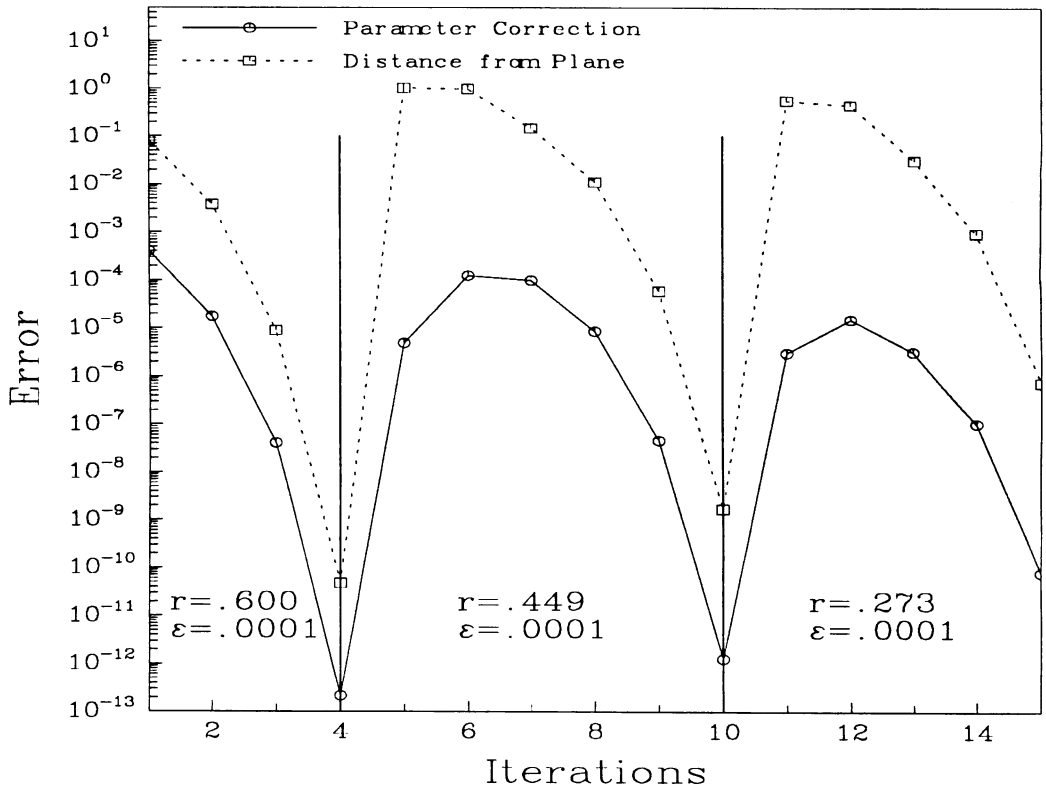

Figure 13: Rate of convergence to the Silnikov connection at $\alpha \sim 35.2741195$.

tween steady states in a more general setting. Their implementation of these algorithms in a version of AUTO will undoubtedly make such calculations routinely possible. Figure 14a shows our approximation of the single pass Silnikov connection ($\alpha \sim 35.2741195$) and 14b shows a nearby limit cycle computed by AUTO (in this case the unstable manifold was actually two dimensional and the stable manifold was one dimensional, but the Silnikov condition was still obeyed).

5 Summary and conclusions

A detailed discussion of the spatio–temporal patterns associated with certain limit cycle solution branches of the KSE has been presented for the parameter interval $0 < \alpha < 40$. A particular space–time symmetry ("Ponies On a Merry-go-round") of one of these branches, its origin and its effect on subsequent bifurcations has also been discussed. We computationally observe that all limit cycle branches studied apparently "terminate" in homoclinic (or heteroclinic) Silnikov connections, involving saddle type steady state solutions. Numerical evidence for the occurrence of a number of features generically as-

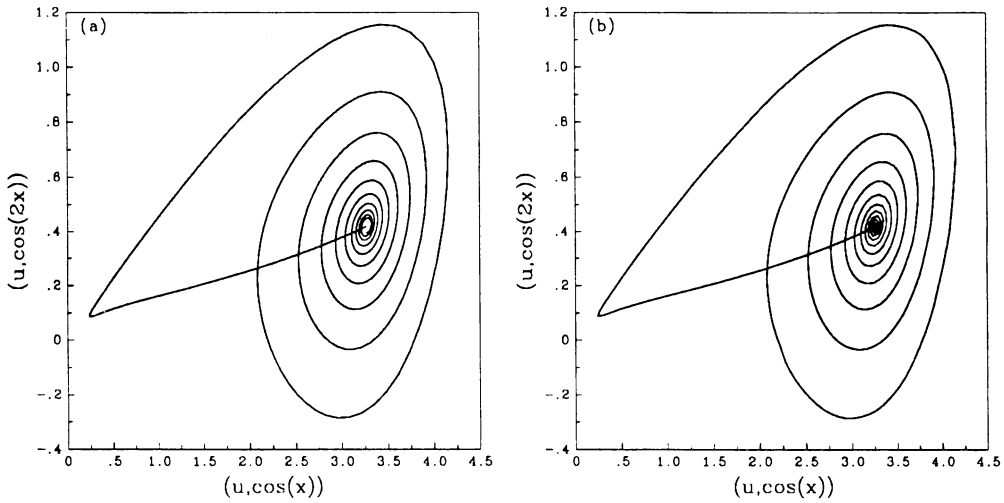

Figure 14: Phase space projections of a converged Silnikov connection ($\alpha = 35.2741195$) and a limit cycle near the the tip of the corkscrew ($\alpha = 35.27398$).

sociated with a Silnikov loop (period doublings, subsidiary homoclinicities, etc.) has also been presented. The minimal phase space dimension consistent with these observations is three; yet a traditional three mode Galerkin truncation of the PDE does not capture this behavior. Exploiting the theory of Approximate Inertial Manifolds (AIMs), we were able to construct a minimal (three dimensional) model capable of qualitatively (and almost quantitatively) reproducing the bifurcation structure.

The sharp reduction in dimensionality allows for the easier visualization of the (approximate) long term dynamics of the PDE; in our three dimensional model the highest dimension of the interacting stable and unstable manifolds of the saddle–focus is two. We exploited this tractable geometry in implementing a simple shooting algorithm to accurately locate the Silnikov connections. More generally, accurate model reduction for PDE discretizations is important in allowing the approximation of (low–dimensional) stable manifolds of steady or oscillatory solutions further away from these solutions in phase space. This should allow for an easier geometric understanding of the phase space structures underlying long term dynamics of the PDE, especially global bifurcations. Our particular example, the KSE, is very well

suited for model reduction using AIMs: dissipation is strong, the first few eigenfunctions of the linear "dissipative" part, used to parameterize the AIM, also happen to be the eigendirections in which the first few instabilities occur and carry most of the energy of the long term solutions. In addition, the spectral implementation of the AIM benefits from the fact that these eigenfunctions are pure Fourier modes. For other PDEs and other geometries, it is quite possible that alternative basis functions (e.g. based on some empirical information about the problem, as is the case in POD) can be much more efficient in parametrizing an appropriate low–dimensional manifold, and hence give rise to an accurate dynamical system of smaller dimension.

Acknowledgements: The work of H.S.B. and I.G.K. was supported in part by NSF Grants CTS–8957213, DMS–8906292 and a David and Lucile Packard Foundation Fellowship; that of M.S.J. was supported in part by NSF grant DMS–9007802. Part of this work was performed while I.G.K. was enjoying the hospitality (and M.S.J. was a postdoctoral member) of the Institute for Mathematics and its Applications at the University of Minnesota.

References

[1] D. Armbruster, J. Guckenheimer, and P. Holmes. Kuramoto–Sivashinsky dynamics on the center–unstable manifold. *SIAM J. Appl. Math.*, 49(3):676–691, June 1989.

[2] D. G. Aronson, M. Golubitsky, and M. Krupa. Ponies on a merry-go-round in large arrays of Josephson junctions. *Nonlinearity (to appear)*, 1991.

[3] P. J. Aston. Introduction to the numerical solution of symmetry–breaking bifurcation problems. In D. Roose, B. DeDier, and A. Spence, editors, *Proceedings on the NATO Advanced Research Workshop on Continuation and Bifurcations: Numerical Techniques and Applications*, pages 139–152. Kluwer Academic Publishers, 1990.

[4] N. Aubry, P. Holmes, J. Lumley, and E. Stone. The dynamics of coherent structures in the wall region of a turbulent boundary layer. *J. F. M.*, 192:115–173, 1988.

[5] W. J. Beyn. Global bifurcations and their numerical computation. In D. Roose, B. DeDier, and A. Spence, editors, *Proceedings on the NATO Advanced Research Workshop on Continuation and Bifurcations: Numerical Techniques and Applications*, pages 169–181. Kluwer Academic Publishers, 1990.

[6] W. J. Beyn. The numerical computation of connecting orbits in dynamical systems. *IMA J. Num. Anal.*, 9:379–405, 1990.

[7] H. S. Brown, M. S. Jolly, I. G. Kevrekidis, and E. S. Titi. Use of approximate inertial manifolds in bifurcation calculations. In D. Roose, B. DeDier, and A. Spence, editors, *Proceedings on the NATO Advanced Research Workshop on Continuation and Bifurcations: Numerical Techniques and Applications*, pages 9–23. Kluwer Academic Publishers, 1990.

[8] H. S. Brown and I. G. Kevrekidis. A numerical study of homoclinic orbits to a saddle–focus and dynamics associated with their existence. *Paper 187e, Presented to the 1990 AIChE annual meeting, Chicago*, 1990.

[9] L. H. Chen and H. C. Chang. Nonlinear waves on thin film surfaces. II. bifurcation analysis of the long–wave equation. *Chem. Eng. Sci.*, 41:2477–2486, 1986.

[10] P. Constantin, C. Foias, B. Nicolaenko, and R. Témam. *Integral Manifolds and Inertial Manifolds for Dissipative Partial Differential Equations.* Appl. Math. Sci., No. 70. Springer–Verlag, 1988.

[11] A. E. Deane, I. G. Kevrekidis, G. E. Karniadakis, and S. A. Orszag. Low dimensional models for complex geometry flows: Application to grooved channels and circular cylinders. *Phys. Fluids A (Submitted)*, 1990.

[12] E. S. Doedel. AUTO: A program for the automatic bifurcation analysis of autonomous systems. *Cong. Num.*, 30:265–284, 1981.

[13] E. S. Doedel. *AUTO 86 User Manual*, February 1986.

[14] E. S. Doedel and M. J. Friedman. Numerical computation of heteroclinic orbits. *J. Comput. and Appl. Math.*, 26:159–170, 1989.

[15] M. J. Friedman and E. Doedel. Numerical computation and continuation of invariant manifolds connecting fixed points with application to computation to combustion fronts. In *Proc. 7th Int. Conf. on Finite Element Methods in flow problems*, April 1989.

[16] M. J. Friedman and E. Doedel. Numerical computation and continuation of invariant manifolds connecting fixed points. *SIAM J. Num. Anal.*, 1991. to appear.

[17] P. Gaspard, R. Kapral, and G. Nicolis. Bifurcation phenomena near homoclinic systems: A two–parameter analysis. *J. Stat. Phys.*, 35(5/6):697–727, 1984.

[18] P. Glendinning and C. Sparrow. Local and global behavior near homoclinic orbits. *J. Stat. Phys.*, 35:645–696, 1984.

[19] J. M. Greene and J. S. Kim. The steady states of the Kuramoto–Sivashinsky equation. *Physica D*, 33:99–120, 1988.

[20] B. Hassard. Computation of invariant manifolds. In P. Holmes, editor, *New Approaches to Nonlinear Problems in Dynamics*, pages 27–42. SIAM, 1980.

[21] J. M. Hyman, B. Nicolaenko, and S. Zaleski. Order and complexity in the Kuramoto–Sivashinsky model of weakly turbulent interfaces. *Physica D*, 23:265–292, 1986.

[22] J. S. Il'yashenko. Global analysis of the phase portrait for the Kuramoto–Sivashinsky equation. Technical Report 665, IMA Preprint, 1990.

[23] M. S. Jolly, I. G. Kevrekidis, and E. S. Titi. Approximate inertial manifolds for the Kuramoto–Sivashinsky equation: Analysis and computations. *Physica D*, 44:38–60, 1990.

[24] I. G. Kevrekidis, H. S. Brown, and M. S. Jolly. Low–dimensional chaos in models of interfacial instabilities: Global bifurcations and the role

of unstable solutions. *Paper 16e, Presented to the 1989 AIChE annual meeting, San Francisco*, 1989.

[25] I. G. Kevrekidis and M. S. Jolly. On the computation of inertial manifolds. *Paper 173c, Presented to the 1988 AIChE annual meeting, Washington*, 1988.

[26] I. G. Kevrekidis, B. Nicolaenko, and J. C. Scovel. Back in the saddle again: A computer assisted study of the Kuramoto–Sivashinsky equation. *SIAM J. Appl. Math.*, 50(3):760–790, 1990.

[27] Y. Kuramoto and T. Tsuzuki. Persistent propagation of concentration waves in dissipative media far from thermal equilibrium. *Prog. Theor. Phys.*, 55(2):356–369, February 1976.

[28] Y. A. Kuznetsov. Computation of invariant manifold bifurcations. In D. Roose, B. DeDier, and A. Spence, editors, *Proceedings on the NATO Advanced Research Workshop on Continuation and Bifurcations: Numerical Techniques and Applications*, pages 183–195. Kluwer Academic Publishers, 1990.

[29] M. Lentini and H. B. Keller. Boundary value problems on semi–infinite intervals and their numerical solution. *SIAM J. Num. Anal.*, 17(4):577–604, August 1980.

[30] J. L. Lumley. The structure of inhomogeneous turbulent flows. In A. M. Yaglom and V. I. Tatarski, editors, *Atmospheric Turbulence and Radio Wave Propagation*, pages 166–178. Moscow: Nauka, 1967.

[31] J. L. Lumley. *Stochastic Tools in Turbulence.* Academic Press, NY, 1970.

[32] M. Luskin and G. Sell. Approximation theories for inertial manifolds. Technical Report 88/76, University of Minnesota Supercomputer Institute, July 1988.

[33] B. Nicolaenko, B. Scheurer, and R. Témam. Some global dynamical properties of the Kuramoto Sivashinsky equation: Nonlinear stability and attractors. *Physica D*, 16:155–183, 1985.

[34] J. C. Scovel, I. G. Kevrekidis, and B. Nicolaenko. Scaling laws and the prediction of bifurcations in systems modeling pattern formation. *Phys. Letters A*, 130:73–80, 1988.

[35] L. Sirovich and C. Sirovich. Low dimensional description of complicated phenomena. *Contemporary Mathematics*, 89:277–365, 1989.

[36] G. I. Sivashinsky. Nonlinear analysis of hydrodynamic instability in laminar flames–I. derivation of basic equations. *Acta Astronautica*, 4:1177–1206, 1977.

[37] C. Sparrow. *The Lorenz Equations: Bifurcations, Chaos and Strange Attractors.* Appl. Math. Sci., No. 41. Springer–Verlag, 1982.

[38] J. W. Swift and K. Wiesenfeld. Suppression of period doubling in symmetric systems. *Phys. Rev. Letters*, 52(9):705–708, February 1984.

[39] E. S. Titi. On approximate inertial manifolds to the Navier–Stokes equations. *J. Math. Anal. Appl.*, 149:540–557, 1990.

Recent IMA Preprints

#	Author/s	Title
699	**László Gerencsér**,	Multiple integrals with respect to L-mixing processes
700	**David Kinderlehrer and Pablo Pedregal**,	Weak convergence of integrands and the Young measure representation
701	**Bo Deng**,	Symbolic dynamics for chaotic systems
702	**P. Galdi, D.D. Joseph, L. Preziosi, S. Rionero**,	Mathematical problems for miscible, incompressible fluids with Korteweg stresses
703	**Charles Collins and Mitchell Luskin**,	Optimal order error estimates for the finite element approximation of the solution of a nonconvex variational problem
704	**Peter Gritzmann and Victor Klee**,	Computational complexity of inner and outer j-radii of polytopes in finite-dimensional normed spaces
705	**A. Ronald Gallant and George Tauchen**,	A nonparametric approach to nonlinear time series analysis: estimation and simulation
706	**H.S. Dumas, J.A. Ellison and A.W. Sáenz**,	Axial channeling in perfect crystals, the continuum model and the method of averaging
707	**M.A. Kaashoek and S.M. Verduyn Lunel**,	Characteristic matrices and spectral properties of evolutionary systems
708	**Xinfu Chen**,	Generation and Propagation of interfaces in reaction diffusion systems
709	**Avner Friedman and Bei Hu**,	Homogenization approach to light scattering from polymer-dispersed liquid crystal films
710	**Yoshihisa Morita and Shuichi Jimbo**,	ODEs on inertial manifolds for reaction-diffusion systems in a singularly perturbed domain with several thin channels
711	**Wenxiong Liu**,	Blow-up behavior for semilinear heat equations:multi-dimensional case
712	**Hi Jun Choe**,	Hölder continuity for solutions of certain degenerate parabolic systems
713	**Hi Jun Choe**,	Regularity for certain degenerate elliptic double obstacle problems
714	**Fernando Reitich**,	On the slow motion of the interface of layered solutions to the scalar Ginzburg–Landau equation
715	**Xinfu Chen and Fernando Reitich**,	Local existence and uniqueness of solutions of the Stefan problem with surface tension and kinetic undercooling
716	**C.C. Lim, J.M. Pimbley, C. Schmeiser and D.W. Schwendeman**,	Rotating waves for semiconductor inverter rings
717	**W. Balser, B.L.J. Braaksma, J.-P. Ramis and Y. Sibuya**,	Multisummability of formal power series solutions of linear ordinary differential equations
718	**Peter J. Olver and Chehrzad Shakiban**,	Dissipative decomposition of partial differential equations
719	**Clark Robinson**,	Homoclinic bifurcation to a transitive attractor of Lorenz type, II
720	**Michelle Schatzman**,	A simple proof of convergence of the QR algorithm for normal matrices without shifts
721	**Ian M. Anderson, Niky Kamran and Peter J. Olver**,	Internal, external and generalized symmetries
722	**C. Foias and J.C. Saut**,	Asymptotic integration of Navier–Stokes equations with potential forces. I
723	**Ling Ma**,	The convergence of semidiscrete methods for a system of reaction-diffusion equations
724	**Adelina Georgescu**,	Models of asymptotic approximation
725	**A. Makagon and H. Salehi**,	On bounded and harmonizable solutions on infinite order arma systems
726	**San-Yih Lin and Yan-Shin Chin**,	An upwind finite-volume scheme with a triangular mesh for conservation laws
727	**J.M. Ball, P.J. Holmes, R.D. James, R.L. Pego & P.J. Swart**,	On the dynamics of fine structure
728	**KangPing Chen and Daniel D. Joseph**,	Lubrication theory and long waves
729	**J.L. Ericksen**,	Local bifurcation theory for thermoelastic Bravais lattices
730	**Mario Taboada and Yuncheng You**,	Some stability results for perturbed semilinear parabolic equations
731	**A.J. Lawrance**,	Local and deletion influence
732	**Bogdan Vernescu**,	Convergence results for the homogenization of flow in fractured porous media
733	**Xinfu Chen and Avner Friedman**,	Mathematical modeling of semiconductor lasers
734	**Yongzhi Xu**,	Scattering of acoustic wave by obstacle in stratified medium
735	**Songmu Zheng**,	Global existence for a thermodynamically consistent model of phase field type
736	**Heinrich Freistühler and E. Bruce Pitman**,	A numerical study of a rotationally degenerate hyperbolic system part I: the Riemann problem
737	**Epifanio G. Virga**,	New variational problems in the statics of liquid crystals
738	**Yoshikazu Giga and Shun'ichi Goto**,	Geometric evolution of phase-boundaries
739	**Ling Ma**,	Large time study of finite element methods for 2D Navier–Stokes equations
740	**Mitchell Luskin and Ling Ma**,	Analysis of the finite element approximation of microstructure in micromagnetics
741	**M. Chipot**,	Numerical analysis of oscillations in nonconvex problems
742	**J. Carrillo and M. Chipot**,	The dam problem with leaky boundary conditions
743	**Eduard Harabetian and Robert Pego**,	Efficient hybrid shock capturing schemes
744	**B.L.J. Braaksma**,	Multisummability and Stokes multipliers of linear meromorphic differential equations

745 **Tae Il Jeon and Tze-Chien Sun**, A central limit theorem for non-linear vector functionals of vector Gaussian processes
746 **Chris Grant**, Solutions to evolution equations with near-equilibrium initial values
747 **Mario Taboada and Yuncheng You**, Invariant manifolds for retarded semilinear wave equations
748 **Peter Rejto and Mario Taboada**, Unique solvability of nonlinear Volterra equations in weighted spaces
749 **Hi Jun Choe**, Holder regularity for the gradient of solutions of certain singular parabolic equations
750 **Jack D. Dockery**, Existence of standing pulse solutions for an excitable activator-inhibitory system
751 **Jack D. Dockery and Roger Lui**, Existence of travelling wave solutions for a bistable evolutionary ecology model
752 **Giovanni Alberti, Luigi Ambrosio and Giuseppe Buttazzo**, Singular perturbation problems with a compact support semilinear term
753 **Emad A. Fatemi**, Numerical schemes for constrained minimization problems
754 **Y. Kuang and H.L. Smith**, Slowly oscillating periodic solutions of autonomous state-dependent delay equations
755 **Emad A. Fatemi**, A new splitting method for scaler conservation laws with stiff source terms
756 **Hi Jun Choe**, A regularity theory for a more general class of quasilinear parabolic partial differential equations and variational inequalities
757 **Haitao Fan**, A vanishing viscosity approach on the dynamics of phase transitions in Van Der Waals fluids
758 **T.A. Osborn and F.H. Molzahn**, The Wigner–Weyl transform on tori and connected graph propagator representations
759 **Avner Friedman and Bei Hu**, A free boundary problem arising in superconductor modeling
760 **Avner Friedman and Wenxiong Liu**, An augmented drift-diffusion model in semiconductor device
761 **Avner Friedman and Miguel A. Herrero**, Extinction and positivity for a system of semilinear parabolic variational inequalities
762 **David Dobson and Avner Friedman**, The time-harmonic Maxwell equations in a doubly periodic structure
763 **Hi Jun Choe**, Interior behaviour of minimizers for certain functionals with nonstandard growth
764 **Vincenzo M. Tortorelli and Epifanio G. Virga**, Axis-symmetric boundary-value problems for nematic liquid crystals with variable degree of orientation
765 **Nikan B. Firoozye and Robert V. Kohn**, Geometric parameters and the relaxation of multiwell energies
766 **Haitao Fan and Marshall Slemrod**, The Riemann problem for systems of conservation laws of mixed type
767 **Joseph D. Fehribach**, Analysis and application of a continuation method for a self-similar coupled Stefan system
768 **C. Foias, M.S. Jolly, I.G. Kevrekidis and E.S. Titi**, Dissipativity of numerical schemes
769 **D.D. Joseph, T.Y.J. Liao and J.-C. Saut**, Kelvin–Helmholtz mechanism for side branching in the displacement of light with heavy fluid under gravity
770 **Chris Grant**, Solutions to evolution equations with near-equilibrium initial values
771 **B. Cockburn, F. Coquel, Ph. LeFloch and C.W. Shu**, Convergence of finite volume methods
772 **N.G. Lloyd and J.M. Pearson**, Computing centre conditions for certain cubic systems
773 **João Palhoto Matos**, Young measures and the absence of fine microstructures in the $\alpha - \beta$ quartz phase transition
774 **L.A. Peletier & W.C. Troy**, Self-similar solutions for infiltration of dopant into semiconductors
775 **H. Scott Dumas and James A. Ellison**, Nekhoroshev's theorem, ergodicity, and the motion of energetic charged particles in crystals
776 **Stathis Filippas and Robert V. Kohn**, Refined asymptotics for the blowup of $u_t - \Delta u = u^p$.
777 **Patricia Bauman, Nicholas C. Owen and Daniel Phillips**, Maximum principles and a priori estimates for an incompressible material in nonlinear elasticity
778 **Patricia Bauman, Nicholas C. Owen and Daniel Phillips**, Maximal smoothness of solutions to certain Euler–Lagrange equations from nonlinear elasticity
779 **Jack Carr and Robert Pego**, Self-similarity in a coarsening model in one dimension
780 **J.M. Greenberg**, The shock generation problem for a discrete gas with short range repulsive forces
781 **George R. Sell and Mario Taboada**, Local dissipativity and attractors for the Kuramoto–Sivashinsky equation in thin 2D domains
782 **T. Subba Rao**, Analysis of nonlinear time series (and chaos) by bispectral methods
783 **Nicholas Baumann, Daniel D. Joseph, Paul Mohr and Yuriko Renardy**, Vortex rings of one fluid in another free fall
784 **Oscar Bruno, Avner Friedman and Fernando Reitich**, Asymptotic behavior for a coalescence problem
785 **Johannes C.C. Nitsche**, Periodic surfaces which are extremal for energy functionals containing curvature functions
786 **F. Abergel and J.L. Bona**, A mathematical theory for viscous, free-surface flows over a perturbed plane
787 **Gunduz Caginalp and Xinfu Chen**, Phase field equations in the singular limit of sharp interface problems
788 **Robert P. Gilbert and Yongzhi Xu**, An inverse problem for harmonic acoustics in stratified oceans
789 **Roger Fosdick and Eric Volkmann**, Normality and convexity of the yield surface in nonlinear plasticity
790 **H.S. Brown, I.G. Kevrekidis and M.S. Jolly**, A minimal model for spatio–temporal patterns in thin film flow